

## Radial resolution enhancement of the NSTX Thomson scattering diagnostic<sup>a)</sup>

B. P. LeBlanc,<sup>b)</sup> A. Diallo, G. Labik, and D. R. Stevens  
*Princeton Plasma Physics Laboratory, Princeton, New Jersey 08543, USA*

(Presented 8 May 2012; received 5 May 2012; accepted 27 June 2012;  
 published online 31 July 2012)

Current magnetic confinement plasma physics research has increased the demand for radial resolution in profile diagnostics, in particular in the edge and pedestal regions. On NSTX, an upgrade of the existing multi-point Thomson scattering diagnostic has been implemented in order to respond to the research program needs. Twelve new radial channels have been added bringing the total number of positions to 42. Four previously un-instrumented fiber bundles were put in service. Eight existing “active” fiber bundles were divided in two sub-bundles each in order to increase spatial resolution. Twelve radial channels now cover the pedestal region with a resolution near one centimeter. Fifteen radial channels cover the core and internal transport barrier regions. Two additional channels were added, one near the inner edge and one in the outer scrape-off layer. The intersection of the focused viewing optics field of view with a finite-width laser beam results in major-radius cross talk between adjacent fiber sub-bundles. A discussion and calculation of the cross talk will be presented. © 2012 American Institute of Physics. [<http://dx.doi.org/10.1063/1.4738655>]

### I. INTRODUCTION

The multi-point Thomson scattering (MPTS) diagnostic system has been providing time dependent  $T_e$  and  $n_e$  profile measurements on NSTX for ten years.<sup>1</sup> A phased implementation continues, made possible by the original installation of key components. For example, the mirror viewing optics has been fully populated with 36 fiber-optics bundles, which are permanently installed; bundle subsets were progressively instrumented as resources became available. Similarly, two of three installed cradles support 30-Hz Nd:YAG lasers. Since 2005, MPTS has been operating with these two lasers, 60-Hz being the routine timing arrangement, and 30 major radius channels stemming from the instrumentation of 29 fiber bundles. The collecting optics views 93% of the machine aperture at the midplane, which includes both sides of the magnetic axis and the outer scrape off layer (SOL). In this paper, we review the implementation of 12 additional radial channels resulting in a total of 42. In response to NSTX’s research program, the radial array was densified primarily at the outer edge transport barrier (ETB) region and new channels were added to the internal transport barrier (ITB) region. Furthermore, two extra channels were added: one near the top in the inner ETB and one more in the SOL. A specially designed fiber-optics holder supports the fiber-bundle array at the focus of the mirror optics viewing along the laser beam path. Spacers between adjacent bundles provide mechanical strength and prevent major-radius viewing overlap. The overlap can result from the intersection of the field of view depth and the finite size laser beam. Thomson scattering (TS) optical arrangements, where the laser beam and collection optics

are on the midplane, are susceptible to major radius overlap. The effect is exacerbated when the beam path is not purely radial as is the case for the MPTS.

### II. INITIAL FIBER OPTICS SPLITTING

The MPTS design provides the option of dividing the output end of a fiber bundle into different branches for increased spatial resolution. In 2005, we tested the idea and “coherently” divided the output end of a fiber bundle into two sub-bundles viewing adjacent sections of the original bundle viewing span. The two branches were assigned to different polychromators. The original 19-fiber bundle was viewing at major radius,  $R$ , of 144 cm. Figure 1 shows before and after photographs obtained through back illumination for a similar division. The conjoint bundles have, respectively, 10 and 9 fibers and view radial spans centered, respectively, at  $R = 144.5$  and 143.6 cm. Subsequent TS measurements during plasma operation revealed that the modification was successful, the two conjoint channels providing meaningful measurements, well tested during the subsequent NSTX experimental campaigns. Figure 2 shows  $T_e$  and  $n_e$  profiles radial overlays at seven times during a Neutral Beam Injection (NBI) plasma: two during the early phase and five during the main discharge. These partial spatial profiles include the ETB and the conjoint radial locations encircled with a dashed line. Let us consider the difference between the inner and outer conjoint radial channels, i.e.,  $\Delta T_e = T_e(R = 143.6 \text{ cm}) - T_e(R = 144.5 \text{ cm})$  and similarly for  $\Delta n_e$ . One can see that for the early times  $\Delta T_e \approx 0$ , but that for the rest of the time  $\Delta T_e \geq 0$ . On the other hand  $\Delta n_e < 0$  during the early times – because of a density profile hollowing – but later on,  $\Delta n_e \geq 0$  during the remainder of the discharge. One can see the ETB moving slightly in and out at various times. We also show a horizontal radial span bar for each position. The latter is computed based on simple

<sup>a)</sup>Contributed paper, published as part of the Proceedings of the 19th Topical Conference on High-Temperature Plasma Diagnostics, Monterey, California, May 2012.

<sup>b)</sup>Author to whom correspondence should be addressed: Electronic mail: leblanc@pppl.gov.

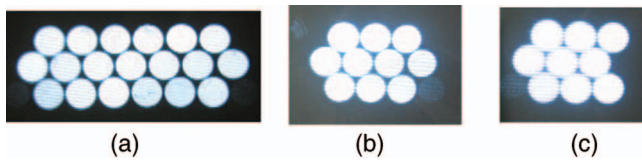


FIG. 1. Fiber bundle splitting, (a) original bundle; (b) 10-fiber sub-bundle; and (c) 9-fiber sub-bundle.

geometric arguments and corresponds to the measurement span along a zero-diameter laser beam. In Fig. 3, we show plots of  $\Delta T_e$  and  $\Delta n_e$ , respectively, against  $T_e$  and  $n_e$ , for a set of 960 measurements obtained during 23 similar-condition discharges to the plasma shown in Fig. 2. Figure 3(a) shows  $\Delta T_e$  with its error  $\delta \Delta T_e$  computed quadratically and similarly for  $\Delta n_e$  in Fig. 3(b). Consistent with observations seen in Fig. 2,  $\Delta T_e \geq 0$  within error bars. On the other hand,  $\Delta n_e$  is slightly negative during profile hollowing, but  $\geq 0$  otherwise. The measured  $\Delta T_e$  and  $\Delta n_e$  are outside of the error bars indicating a low level of radial cross talk. In fact the conjoint channels have been validated over thousands of plasma discharges and have provided routinely meaningful data since their installation.

### III. RADIAL RESOLUTION ENHANCEMENT

Based on the success of the “original” fiber bundle division, it was decided to continue using this technique to improve spatial resolution. As mentioned earlier, 36 full fiber bundles – comprising 19 fibers – are permanently in place, but until recently only 29 of them had been instrumented. Eight of the latter have been split in two for the current 42-channel upgrade, which also includes the instrumentation of four previously unused full fiber bundles. This implementation adds 12 new radial channels for a total of 42 spatial positions. The spatial allocation of new channels was done in response to the demands of the research team. We can see in Fig. 4 an overlay

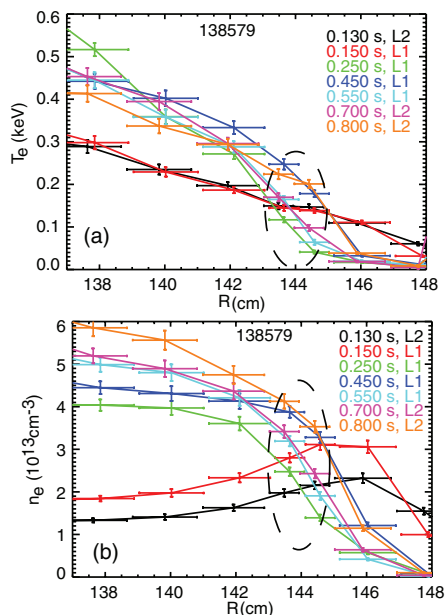


FIG. 2. Thomson scattering measurements at seven times: (a)  $T_e$  and (b)  $n_e$ . Conjoint radial locations circled with a dashed line.

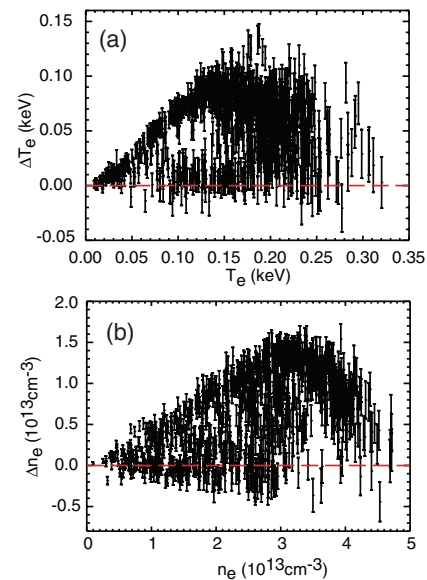


FIG. 3. Measurement difference in  $T_e$  and  $n_e$  between conjoint channels: (a)  $\Delta T_e$ ; (b)  $\Delta n_e$ . Data shown against  $T_e$  or  $n_e$  at  $R = 143.6$  cm.

of the center to center distance,  $dR_{cc}$ , between adjacent radial channels for 30-channel and the 42 channel arrangements. In the latter case, 33 fiber bundles are utilized: 24 full bundles and 9 divided into 18 sub-bundles. Special attention was given to the ETB, which now has 12 consecutive fiber sub-bundles. The spatial resolution of the ITB has also been improved, with a total of 15 channels. Finally, two new channels were added: one at the inner ETB and one more to the SOL.

Because no spacer separates the conjoint channel pairs, an estimate of radial overlap in the measurement needs to be done. In the past MPTS has been supplying profile results with one-sigma “vertical” error bars for  $T_e$ ,  $n_e$ , and electron pressure  $p_e$ . But it also supplied an estimate of the major radial span over which the measurement occurs. The latter is based on one-dimensional estimates of the laser scattering length for each radial position. As for the first conjoint radial pair mentioned above, the radial span of each sub-bundle has been given a long lived temporary approximation of half of the full bundle radial span. In the following, we proceed to improved calculations in preparation for 42-channel MPTS operation on NSTX-U.<sup>2</sup> One can see in Fig. 5 the geometry

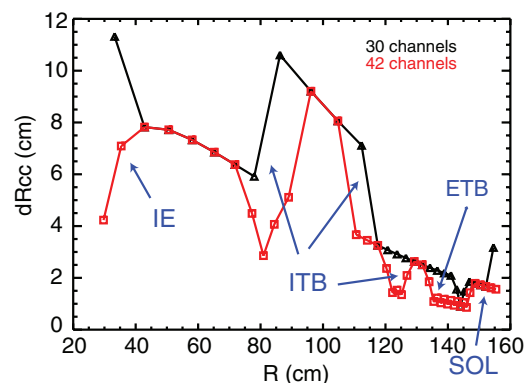


FIG. 4. Spatial position center to center distances for 30-channel and 42-channel configurations.

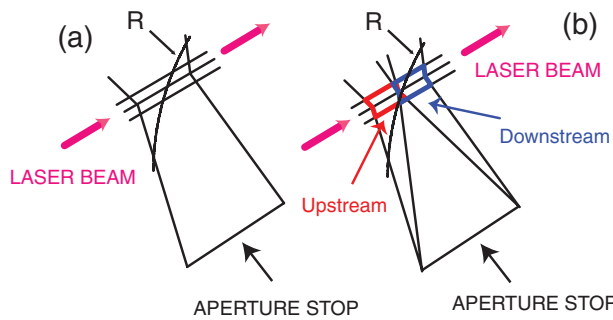


FIG. 5. Schematic illustration of major radius overlap: (a) fiber bundle before division; (b) conjoint sub-bundles after division. Drawing is not to scale.

corresponding to fiber bundle division. The view is looking down at the midplane intersection of the viewing optics ray traces and a finite-diameter laser beam. The direction of the laser beam propagation is indicated by a magenta arrow. The full bundle geometry is seen in panel (a) and that of a divided bundle is seen in panel (b). An irregular hexagon marks the perimeter of the laser-and-optics intersection for each sub-bundle. In Fig. 6, we show a scaled drawing of the geometry for the innermost split fiber bundle. The nominal major radius is  $R \approx 80$  cm. We use the letters “u” and “d” to tag parameters corresponding to upstream and downstream of the laser beam propagation. One can see sectors corresponding to circles of different major radius values. The sectors appear as straight lines on this scale, which are not at right angles with the laser direction, consistent with the MPTS geometry. The calculations can be divided into two parts: (1) using the geometrical extrema of the hexagons; (2) distributing evenly a set of points within each of the hexagons and calculating average and standard deviation. In the geometric calculation, one computes the average major radius of the upstream bundles as the average of the largest and smallest major radii found among the hexagon vertices. If  $R_{hex}$  is the set of major radii corresponding to the six vertices of the upstream hexagon, then we can write the geometrically defined upstream major radius as  $R_{ug} = (\text{Max}(R_{hex}) + \text{Min}(R_{hex}))/2$  and its half span as  $dR_{ug} = (\text{Max}(R_{hex}) - \text{Min}(R_{hex}))/2$ . Similar definitions can be made for the downstream geometrically derived parameters  $R_{dg}$  and  $dR_{dg}$ .

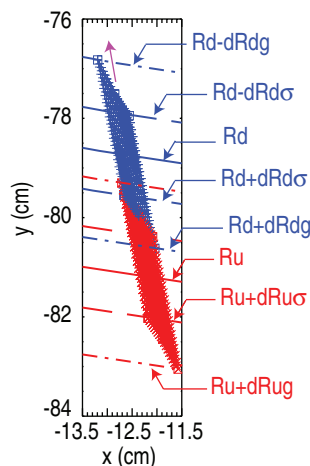


FIG. 6. Geometry for innermost fiber division. Nominal  $R \approx 80$  cm.

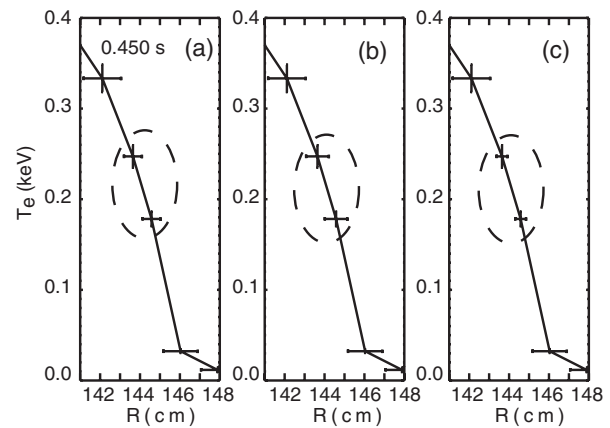


FIG. 7. Comparison of radial span evaluation: (a) current, (b) extrema, and (c) distribution, shown inside dashed circles.

In the second computation,  $N_{dist} = 400$  points are evenly distributed within each of the upstream and downstream hexagons. We compute the corresponding set of major radii  $R_{dist}$ . These points can be seen in Fig. 6. If  $R_{dist}$  corresponds to upstream distribution, then one computes the average  $R_{u\sigma} = \sum R_{dist}/N_{dist}$  and the standard deviation  $dR_{u\sigma}$  for the upstream hexagon. The calculations for  $R_{d\sigma}$  and  $dR_{d\sigma}$  follow in a straightforward manner for the downstream section. The calculations of  $R_{ug}$  and  $R_{u\sigma}$  give essentially the same results: within less than 1 mm over most of the radial profile. For this reason, we simply use  $R_u$  and  $R_d$  in Fig. 6. Hence we see sectors with respective radius  $R_u$  and  $R_d$  corresponding to the upstream and downstream major radii. Also shown in the figure are sectors with radii  $R_d \pm dR_{dg}$  corresponding to the extrema edges of the downstream geometry. Similar sectors are also drawn for the upstream geometry, although not all sectors are labeled to help visibility. We also show upstream and downstream sectors with radii  $R_u \pm dR_{u\sigma}$  and  $R_d \pm dR_{d\sigma}$ . These correspond to one-sigma standard deviation among the distributed points discussed above. The one-sigma radial span values are about half of the geometrical extrema calculation. While we intend to continue providing the MPTS profile data with its current “dR” based on the one-dimensional laser scattering length, we are considering adding the one-sigma evaluation as well, since it would be a better match to the one-sigma “vertical” error bars provided for  $T_e$ ,  $n_e$ , and  $p_e$  profiles. The radial overlap, expressed as a fraction of a sub-bundle radial span, varies from 0.24 to 0.34 when based on extrema calculations; it is nonexistent based on the one-sigma radial span. We can see in Fig. 7 a side-by-side comparison of the three radial span calculations: (a) current, (b) extrema, and (c) distribution. The calculation used currently falls between the extrema and distribution (one-sigma) evaluations.

## ACKNOWLEDGMENTS

This work is supported by U.S. Department of Energy Contract No. DE-AC02-09CH11466.

- <sup>1</sup>B. P. LeBlanc, *Rev. Sci. Instrum.* **74**, 1659 (2003) and references therein.
- <sup>2</sup>A. Diallo, B. P. LeBlanc, G. Labik, and D. Stevens, “Prospects for the Thomson Scattering System on NSTX-Upgrade,” *Rev. Sci. Instrum.* (these proceedings).